International Journal of Technology 15(2) 432-441 (2024)
Received July 2023 / Revised September 2023 / Accepted November 2023

International Journal of Technology

Novel Multiphase CO_2 Photocatalysis System Using N-TiO_2/CNCs and CO_2 Nanobubble

Haroki Madani[1], Arie Wibowo[2,3], Dwiwahju Sasongko[1], Manabu Miyamoto[4], Shigeyuki Uemiya[4], Yogi Wibisono Budhi[1,3,5*]

[1]*Department of Chemical Engineering, Institut Teknologi Bandung, Jl. Ganesha 10, Bandung, 40132, Indonesia*
[2]*Material Science and Engineering Research Group, Faculty of Mechanical and Aerospace Engineering, Institut Teknologi Bandung, Jl. Ganesha 10, Bandung, 40132 Indonesia*
[3]*Research Center for Nanoscience and Nanotechnology, Institut Teknologi Bandung, Jl. Ganesha 10, Bandung, 40132, Indonesia*
[4]*Department of Chemistry and Biomolecular Science, Gifu University, 1-1 Yanagido, 501-1193 Gifu, Japan*
[5]*Research Group of Chemical Engineering Process Intensification, Institut Teknologi Bandung, Jl. Ganesha 10, Bandung, 40132, Indonesia*

Abstract. In this study, a novel CO_2 photocatalysis system was developed by modifying TiO_2 as a photocatalyst and introducing CO_2 nanobubble to the system. TiO_2 photocatalyst is modified by adding CNCs as support to increase the surface area and adding nitrogen doping to reduce the band gap and minimize electron–hole recombination. CO_2 nanobubbles are introduced to increase the surface area between the CO_2 gas and liquid phases to reduce mass transfer limitations. Thus, the amount of CO_2 in the liquid phase increases. Nanobubbles have been successfully generated by the hydrodynamic cavitation method, which produces bubbles with two size clusters, namely 200–400 nm, which belong to nanobubbles, and 2–10 um, which belong to microbubbles. The TiO_2 has an anatase phase and crystallite size of 20.90 nm for TiO_2/CNCs and 19.20 nm for N-TiO_2/CNCs. The activity test without nitrogen doping produced a methanol product of 0.77 mmol/g catalyst, which shows that this multiphase CO_2 photocatalytic system is feasible for CO_2 photocatalytic reactions. The addition of nitrogen doping succeeded in reducing the band gap from 3.20 eV to 3.10 eV and increasing the methanol yield. The photocatalysis activity test with N-doped TiO_2/CNCs resulted in a higher methanol yield, which is 1.13 mmol/g catalyst under UV-C irradiation for 6 hours.

Keywords: CO_2 photocatalysis; Multiphase reaction; Nanobubble; Nitrogen doping; TiO_2

1. Introduction

CO_2 photocatalysis is an appealing solution to reduce CO_2 on the earth's surface because this method not only can reduce CO_2 but also can provide solar fuels (CH_4, CH_3OH, HCHO, HCOOH) as an alternative to fossil energy (Shao *et al.,* 2022). TiO_2 is the most used semiconductor for CO_2 photocatalysis due to its non-toxic characteristics, high energy potential, and low cost. However, TiO_2 has a low photoconversion rate due to its high band gap, which results in a high energy requirement for electron excitation, electron-hole recombination, a low ability to absorb sunlight, and a low ability to adsorb CO_2 (Low, Cheng, and Yu, 2017). Thus, TiO_2 needs to be modified further to improve its performance

*Corresponding author's email: y.wibisono@itb.ac.id, Tel.: +62-22-2500989;
doi: 10.14716/ijtech.v15i2.6694

so that the photocatalytic reaction becomes more efficient.

TiO_2 can be modified in various ways, such as the addition of co-catalysts and doping. The effects of co-catalysts and doping can vary based on the type of atom used. Some examples of co-catalysts are Ag, Co, and Cu. The addition of a plasmonic Ag metal core can increase the photon flux on TiO_2, which can increase the CO_2 photocatalysis conversion (Hong *et al.,* 2019). A co-based co-catalyst can increase CO_2 adsorption capacity and provide more CO_2 in the reaction (Zhang *et al.,* 2020). Cu co-catalyst is more beneficial for CO_2 adsorption and a good co-catalyst for improving catalytic selectivity to CH_3OH (Xi *et al.,* 2022). Doping is another type of TiO_2 modification that can use metal or non-metal atoms as dopants. The addition of dopant didn't lead to a structural defect that occurs in co-catalyst modification, which is an advantage of doping modification if compared with co-catalyst. An example of TiO_2 modification with doping is using N and Mo. N-doping can reduce the band gap and minimize electron-hole recombination. In addition to lowering the band gap, nitrogen doping can minimize electron-hole recombination by filling the oxygen defect in TiO_2, which is the key recombination site (Kumar, Das, and Deepa, 2020). Mo-doping can increase the selectivity toward CH_4 products and increase electron-hole separation and proton supply (Feng *et al.,* 2020). A smaller band gap allows electrons to be excited by lower energy light so that photocatalysts can be used in visible light irradiation. For example, as Kumar, Das, and Deepa (2020) reported, nitrogen doping can lower the band gap of TiO_2/CdS from 3.17 eV to 2.91 eV.

Besides using co-catalyst and doping, TiO_2 can also be modified by creating a mesoporous structure, which can increase the active site of the photocatalyst. For example, Yudha *et al.* (2020) use dammar-gum as a soft template for mesoporous TiO_2 synthesis. Another interesting material that can be used for mesoporous TiO_2 templates is cellulose nanocrystals (CNCs) (Chen *et al.,* 2016). CNCs are cellulose-based nanomaterial with high crystallinity, between 54–88% (Moon *et al.,* 2011). CNCs are renewable materials that can be made from various sources containing cellulose, such as wood (Leung *et al.,* 2011), flax (Leung *et al.,* 2011), empty palm oil bunch (Harahap *et al.,* 2023; Marpongahtun *et al.,* 2023; Budhi *et al.,* 2018; Wibowo *et al.,* 2018), and other lignocellulosic materials (Restiawaty *et al.,* 2022). Even CNCs can be produced from waste materials containing cellulose, such as paper and denim waste (Culsum *et al.,* 2021). CNCs have several superior properties, such as high mechanical properties, high surface area, high biocompatibility, and low toxicity (Brinchi *et al.,* 2013). With renewable sources of raw materials and superior properties, CNCs can be a long-term alternative green material for various purposes. CNCs can be used as a material to support various catalysts, one of which is TiO_2. Maimaiti *et al.* (2019) conducted a study related to TiO_2 photocatalysts dispersed on the surface of CNCs with the addition of EDA treatment. The photocatalyst produced 4.5 times more products than pure TiO_2 (P25) photocatalyst. The small size of CNCs causes a large surface area that increases the surface area of the TiO_2 photocatalyst active center. With many active centers, the number of products produced is also greater.

Besides photocatalyst modification, CO_2 photocatalytic conversion can also be increased by improving the photocatalytic process. In multiphase system, the mass transfer limitation become a hindrance for CO_2 conversion. To overcome the issue of CO_2 mass transfer limitation in a multiphase system, reducing the bubble size to the smallest possible can increase the contact surface area between the gas and liquid phases. In addition, the smaller bubble size can produce a larger mass transfer coefficient (k_La) so that the mass transfer of CO_2 from the gas phase to the liquid phase becomes faster. Nanobubbles are defined as gas bubbles that have a diameter smaller than 1000 nm. The use of nanobubbles over regular bubbles in a process has various advantages, including high mass transfer

efficiency, high bubble stability, and low rising velocity (Ulatowski *et al.,* 2019). The utilization of nanobubble in chemical reactions remains relatively limited. Nevertheless, its application exhibits considerable potential. For example, Mase *et al.* (2013) reported a significant enhancement in the conversion rate from 2% to 99% in the hydrogenation of alkenes through the usage of nanobubble.

In this study, a CO_2 photocatalysis reaction is carried out using CO_2 nanobubble as the source of CO_2. This is expected to increase the contact surface area of the gas and liquid phases and increase the CO_2 mass transfer coefficient. Besides, TiO_2 is modified by dispersing it on the CNC surface and adding nitrogen doping. Nitrogen doping is expected to lower the band gap and minimize the electron-hole recombination so that more electrons are utilized for CO_2 reduction, leading to higher CO_2 conversion. The aim of this study is to study the feasibility of CO_2 nanobubble usage in multiphase CO_2 photocatalysis reaction in a batch reactor without the in and out flow of CO_2 gas. We believe that the result of this study can open new possibilities in the development of CO_2 photocatalysis reactions.

2. Methods

2.1. Materials

Titanium tetra isopropoxide (TTIP, 97.0%), ethanol absolute (99.99%), nitric acid (69%), triethylamine, and sodium hydroxide (50%) were purchased from Merck kGaA, Darmstadt, Germany. Cellulose nanocrystals (CNCs) were purchased from Celluforce, Quebec, Canada. Deionized water was used in all experiments.

2.2. Photocatalyst Synthesis

The TiO_2 photocatalyst was synthesized by the sol-gel method under ambient conditions using TTIP as a precursor. While stirred continuously, 1.2 ml of TTIP was mixed with 20 ml of absolute ethanol. 20 mL of Nitric Acid (0.1 M) was added to the mixture and then continued with the addition of 1 g of cellulose nanocrystals (CNCs) under vigorous stirring for 10 minutes. NaOH 0.2 M solution was added dropwise until the mixture reached a pH of 4. The mixture becomes more viscous at this stage and a gradual color change occurs from transparent to white. The mixture was then left for 24 hours to undergo the aging process. After aging, the mixture was centrifuged 3 times at 6000 rpm and finally dried at 70°C for 12 hours. The resulting white solid is referred to as TiO_2/CNCs photocatalyst. To obtain N-TiO_2/CNCs, 0.8 mL of triethylamine (TEA) was added to the mixture prior to the addition of NaOH solution. The synthesis procedure scheme of TiO_2/CNCs and N-TiO_2/CNCs are presented in Figure 1.

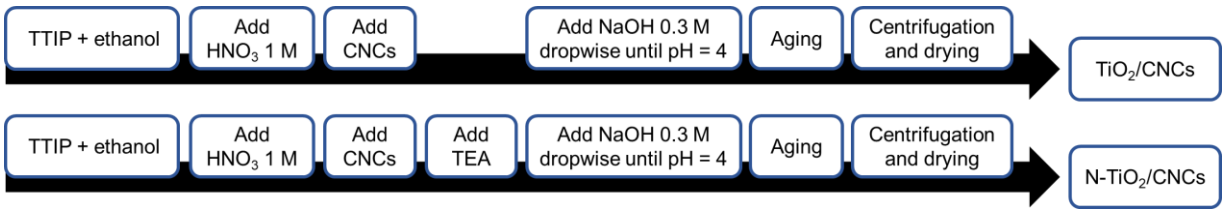

Figure 1 Photocatalyst synthesis procedure

2.3. Photocatalyst Characterization

TiO_2/CNCs and N-TiO_2/CNCs photocatalysts were examined by X-ray diffraction (Bruker D8 Advance, Japan) using Cu Kα radiation, with an accelerating voltage of 16 kV and a current of 30 mA. The characteristic peaks of anatase [101] peak at 2θ = 25°, brookite [121] at 2θ = 31°, and rutile [110] at 2θ = 27°, respectively, were used to estimate the crystallite size of the samples. Scanning electron microscopy (SU-3500, Japan) was used to study the morphology of the TiO_2/CNCs powders at a working distance of 8 mm with an

accelerating voltage and current of 30 kV and 100 mA, respectively. High-resolution transmission electron microscopy (HRTEM, H9500, Japan) was used to study the particle size and distribution. UV-Vis diffuse reflectance spectra (DR UV-Vis) of the prepared samples were measured by a UV-Vis spectrophotometer (UV-2600, Shimadzu) with an integrating sphere attachment ranging from 200 to 800 nm, and TiO_2 was used as a reflectance standard. The band gap energy (E_g) for the direct band gap semiconductor was evaluated using the Kubelka-Munk function as presented in Equation 1.

$$f\left(R_\infty\right)=\frac{k}{s}=\frac{\left(1-R\right)^2}{2R} \quad (1)$$

where $f(R\infty)$ is the Kubelka-Munk function, k is the absorption coefficient, s is the scattering coefficient, and R is the surface reflectance.

2.4. Nanobubble Generation and Photocatalytic Activity Test

CO_2 nanobubbles were generated by the hydrodynamic cavitation method using a nanobubble generator from Nanobubble.id with the type of NB S1. The according to the system depicted in Figure 2a. During the generating process, the temperature was kept below 28°C. Water was pumped into the main container to create a circulation from the main container to the nanobubble generator and vice versa. The CO_2 gas with 0.1 LPM flow rate was injected into the nanobubble generator via the water that passed through it. After 1 hour of nanobubble generation, the water in the main container was either stored for characterization or utilized in CO_2 photocatalysis. The characterization of nanobubble is carried out by dynamic light scattering (DLS) to analyze nanobubble size and its distribution.

The photocatalytic activity test was carried out in a batch reactor, as illustrated in Figure 2b. The reactor was filled with 200 mL of water containing generated nanobubble and 0.2 g of photocatalyst. The mixture in the reactor was stirred at 300 rpm during the reaction process. The photocatalysis was carried out by irradiating the reactor using a UV lamp (UV-C, 15 W, 280 nm) or visible lamp (15 W, 580–750 nm) on both sides, as illustrated in Figure 2b. The reaction was carried out for 6 hours, and the sample of liquid product was taken to be analyzed using Gas Chromatography with Porapack Q column. All the CO_2 used in this system is sourced exclusively from pre-generated CO_2 nanobubbles. However, there is a drawback to this setup as the product yield is limited due to the finite supply of available CO_2. Nevertheless, this system was intentionally designed to showcase the significance of CO_2 nanobubbles in the photocatalytic conversion of CO_2 into solar fuel.

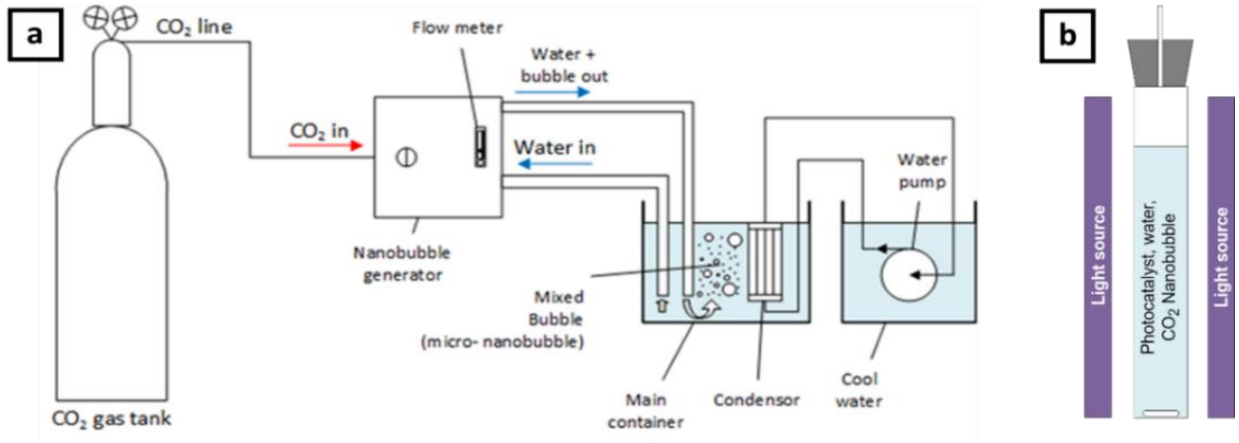

Figure 2 (a) Nanobubble generation system for CO_2 nanobubble generation and (b) CO_2 photocatalysis batch reactor using nanobubble

3. Results and Discussion

3.1. Visual Observation of Photocatalyst Synthesis

TiO_2/CNCs synthesis processes can be separated into four steps: 1) TTIP mixing with solvent, 2) HNO_3 to lower the pH, 3) NaOH addition, and 4) aging. The visual observation of each step is presented in Figure 3.

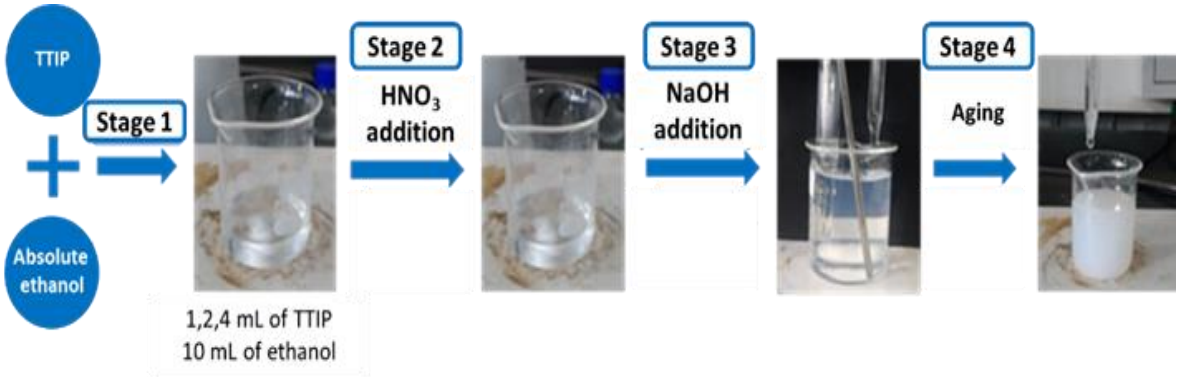

Figure 3 Visual observation of Photocatalyst Synthesis through the sol-gel method

In the first step, TTIP was mixed into absolute ethanol with a purity of 99.99% and followed by HNO_3 1 M addition to avoid uncontrolled formation of $Ti(OH)_4$ due to the hygroscopic nature of TTIP. $Ti(OH)_4$ particles were formed during the hydrolysis of TTIP, which was triggered by the gradual addition of NaOH (Mustapha *et al.*, 2020). The hydrolysis process was then followed by a condensation process that occurred during the aging stage, which took 24 hours. In this stage, the $Ti(OH)_4$ was converted to TiO_2 while producing water. As reported by Martakov *et al.* (2018), during the aging stage, not only does the formation of TiO_2 occur, but also the deposition of TiO_2 on the surface of the CNCs. The deposition of TiO_2 on the surface of TiO_2 occurs through electrostatic and chemical interaction. The electrostatic interaction is triggered by the positive surface charge on TiO_2 particles and the negative surface charge on the CNCs surface due to the existence of hydroxyl groups. The chemical interaction between TiO_2 and CNCs occurs in the form of hydrogen bonds between TiO_2 and hydroxyl groups on the surface of CNCs.

3.2. Photocatalyst Characterization

Several characterizations were carried out to confirm the presence of TiO_2 on the surface of the CNCs, namely TEM, XRD, and DR UV-Vis. Figure 4 shows the CNCs and TiO_2/CNCs under TEM observation.

TEM characterization results show that CNCs and TiO_2/CNCs have needle-like shapes. The average diameter and length of the CNCs particles are 30.30 ± 7.90 nm and 299 ± 67 nm, respectively, as determined from the analysis results using ImageJ software. Although the CNCs and TiO_2/CNCs particles have a common shape, the two have differences when viewed from the edges. On TiO_2/CNCs, black spots are suspected to be TiO_2 particles attached to the surface of the CNCs. Further confirmation of the presence of TiO_2 can be seen from the results of the XRD characterization, as presented in Figure 4c.

The CNCs sample showed peaks of 2θ at 15°, 17°, 23°, and 34°, which indicated that the cellulose contained in the CNCs was type I cellulose. In detail, each of these peaks successively represents the crystallographic plane of (1 0 1), (1 0 -1), (0 0 2), and (0 0 4) (Jiang *et al.*, 2017). Meanwhile, the TiO_2 sample showed 2θ peaks at 24.9°, 37.6°, 47.8°, 53.7°, 62.5°, 68.5°, 70.1° and 74.88° which represents the crystallographic plane of (1 0 1), (0 0 4), (2 0 0), (1 0 5), (2 0 4), (1 1 6), (2 2 0) and (2 1 5). These peaks are in good agreement with anatase TiO_2 peaks based on JCPDS no. 21-1272.

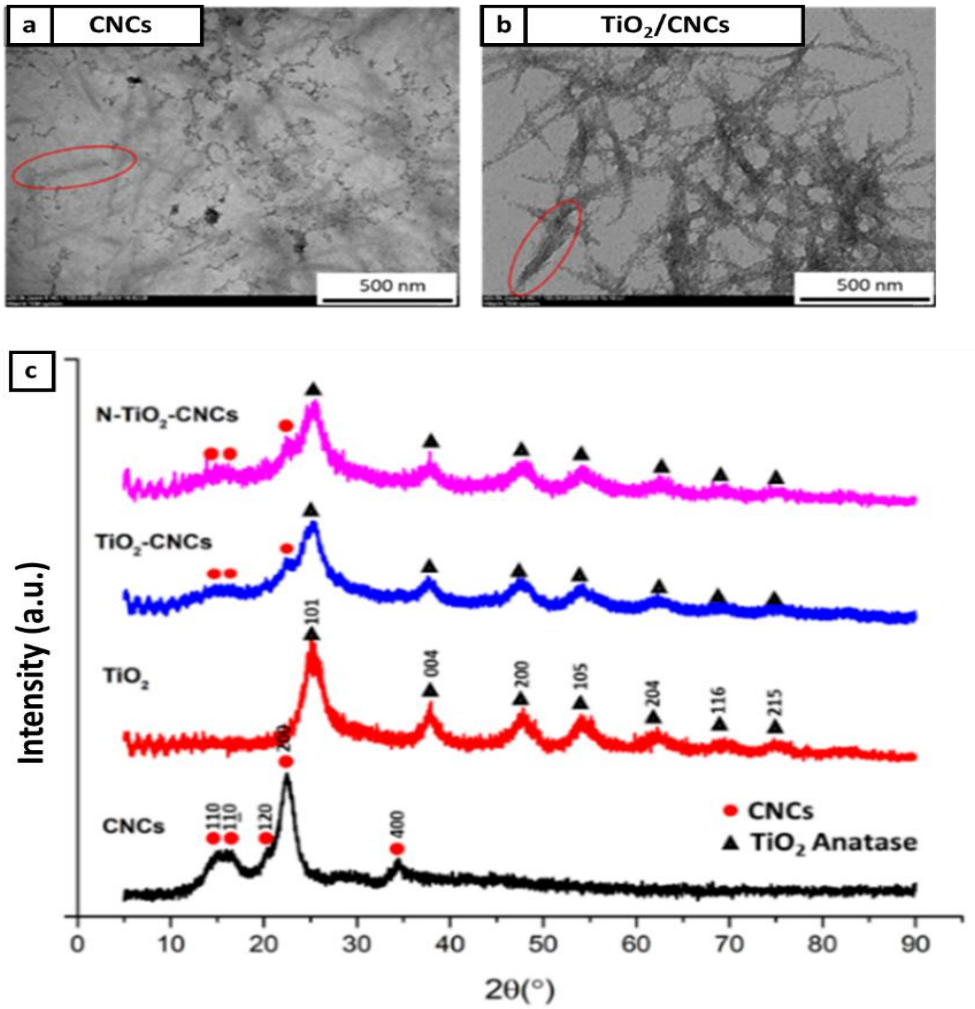

Figure 4 (a,b) TEM observations and (c) XRD curve of CNCs and TiO_2/CNCs

DR UV-Vis is another method that can confirm the presence of TiO_2 and estimate the band gap of the photocatalyst. Figure 5 shows the results of the reflectance curves and Kubelka-Munk Plot of CNCs, TiO_2, and TiO_2/CNCs.

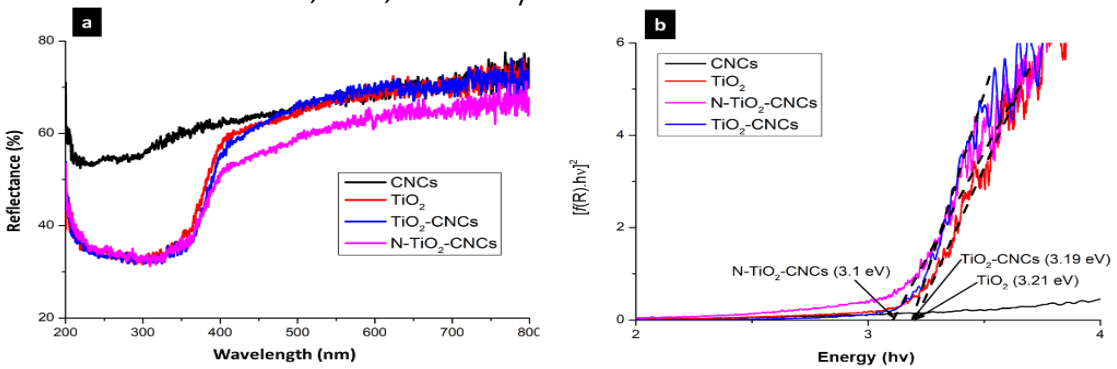

Figure 5 (a) Reflectance curve and (b) Kubelka-Munk Plot of CNCs, TiO_2, TiO_2/CNCs, and N-TiO_2/CNCs

As depicted in Figure 5, CNCs exhibit a relatively straight reflectance curve, suggesting that there is no dominant light absorption activity at a specific wavelength. This is expected since CNCs are not semiconductor materials capable of exciting electrons when exposed to light at a particular wavelength. In contrast, TiO_2 and TiO_2/CNCs have a lower reflectance at a 200–400 nm wavelength, meaning that more light is absorbed in that area. In other

words, TiO_2 and TiO_2/CNCs can excite electrons in irradiating light with a wavelength below 400 nm. This wavelength is equivalent to a band gap energy of ~3.2 eV, which is the band gap of TiO_2 (Mustapha *et al.,* 2020). From Kubelka-Munk Plot, the TiO_2 and TiO_2/CNCs samples have a band gap of 3.21 and 3.19 eV, respectively. The N-TiO_2/CNCs photocatalyst has a band gap of 3.1 eV, which is lower than TiO_2/CNCs. This result confirms that nitrogen doping can lower the band gap energy and enable the photocatalyst to be used under visible light irradiation.

3.3. Nanobubble Characterization

Figure 6 shows the visual observation of the water before and after the nanobubble generation.

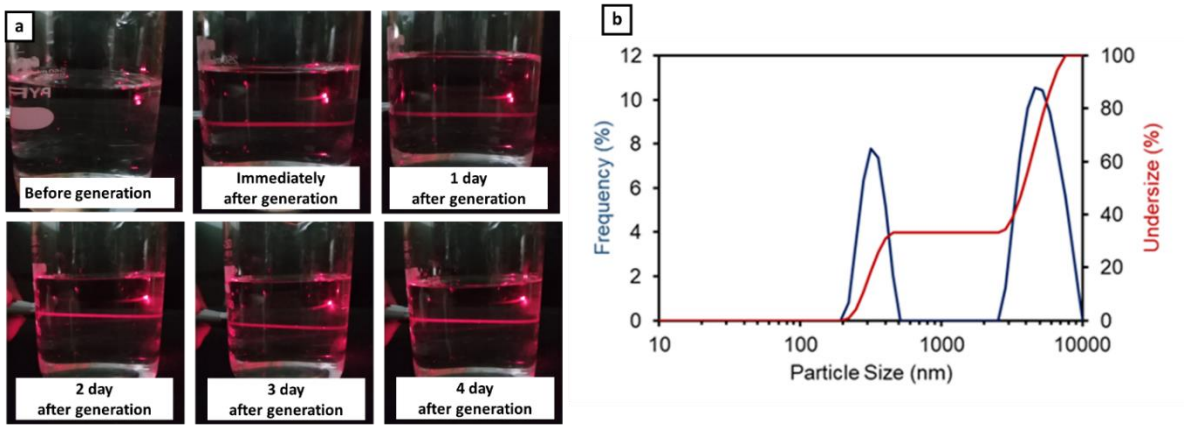

Figure 6 Nanobubble characterization results: (a) Visual observation; (b) Dynamic Light Scattering (DLS) result

Nanobubble has high stability because it has a very long rising time. In comparison, the rising time of nanobubble particles can be days or even months (Ulatowski *et al.,* 2019), while microbubbles and macrobubbles, respectively, have rising times in the range of minutes and seconds (Temesgen *et al.,* 2017). Figure 6a shows that CO_2 nanobubble still remained in the water after 4 days, which is an important justification for the usage of CO_2 nanobubble in batch reactors after its generation.According to the DLS results in Figure 6b, the generated CO_2 nanobubbles exhibit two size clusters, categorized as nanobubbles with a size of 200–400 nm and microbubbles with a size of 2–10 µm. Based on the plot of undersize (y-axis on the right) vs particle size, 35% of the total generated nanobubbles are below 400 nm in size.

3.4. Photocatalyst Activity Test of TiO_2/CNCs

The photocatalytic activity test was carried out at room temperature with a UV-C lamp and visible light in a batch reactor for 6 hours. Figure 7 shows the GC curve of the liquid product resulting from CO_2 photocatalysis with TiO_2/CNCs photocatalyst.

Based on Figure 7a, the liquid product of CO_2 photocatalysis has two peaks at 1.1 and 2 minutes, which are the retention times for water and methanol, respectively. In detail, the resulting methanol product was 0.77 mmol/g catalyst for TiO_2/CNCs and 1.13 mmol/g catalyst for N-TiO_2/CNCs. The existence of methanol in CO_2 photocatalysis products at least proves two things. First, TiO_2/CNCs and N-TiO_2/CNCs photocatalyst has photocatalytic activity under UV-C light, so the photocatalysis reaction can occur. Second, the proposed system using CO_2 nanobubble is feasible for CO_2 photocatalysis in multiphase reactions. An important point to highlight from this result is that there was no CO_2 gas flow during the photocatalysis reaction. All CO_2 utilized during the reaction solely originated from CO_2 nanobubbles pre-existing in the system before the reaction.

Figure 7b shows the comparison of TiO_2/CNCs (undoped) and N-TiO_2/CNCs (N-doped) photocatalysts under visible light irradiation. It is shown that the doped photocatalyst exhibits visible light photocatalytic activity while the undoped does not. This is due to the lower band gap energy of N-TiO_2/CNCs, so visible light with lower energy can excite the electron in the doped photocatalyst. From the Kubelka-Munk Plot that has been discussed earlier, N-TiO_2/CNCs have a band gap of 3.1 eV. Based on the Planck equation (E (eV) = 1240/λ (nm)), 3.1 eV is equivalent to the wavelength of 400 nm, which belongs to visible light. In comparison, Kumar, Das, and Deepa (2020) reported that nitrogen doping addition to TiO_2/CdS can reduce the band gap from 3.17 eV to 2.91 eV (Kumar, Das, and Deepa, 2020).

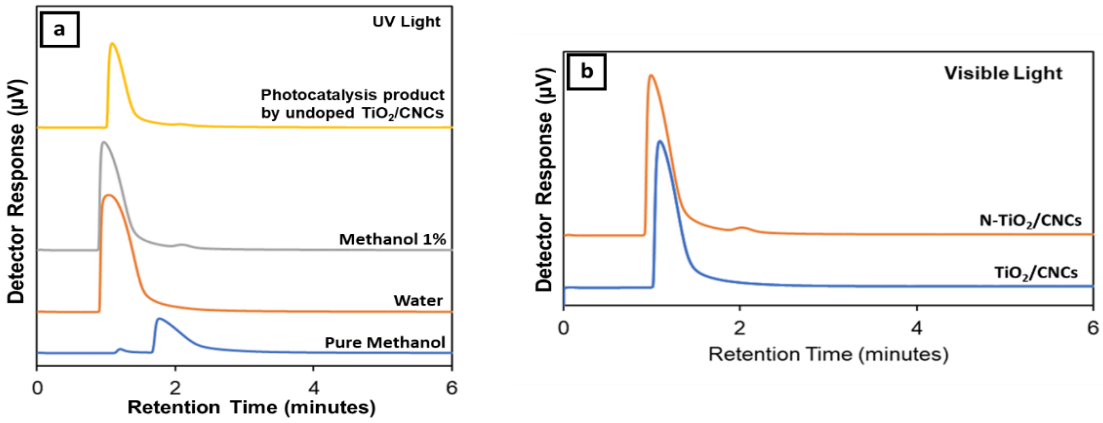

Figure 7 GC curve of liquid product produced from CO_2 photocatalysis by TiO_2/CNCs photocatalyst at (a) UV-C light and (b) visible light

4. Conclusions

In this study, the photocatalysis reaction of CO_2 was carried out in a batch reactor, where CO_2 gas in the form of nanobubbles in water was directly irradiated with light. There is no flow of CO_2 gas in and out. All CO_2 used for the reaction was provided from nanobubbles in the water. The presence of methanol in the photocatalysis product with this system proves the feasibility of multiphase systems with CO_2 nanobubbles for CO_2 photocatalytic reactions. Nitrogen doping to the photocatalyst reduced the band gap from 3.20 eV to 3.10 eV, which was later proven by the photocatalytic activity of N-TiO_2/CNCs under visible light irradiation.

Acknowledgments

The authors acknowledge the Ministry of Education, Culture, Research, and Technology of the Republic of Indonesia for providing financial support through the National Competitive Research-Doctoral Dissertation Research Scheme (contract number: 110/E5/PG.02.00.PL/2023; 318/IT1.B07.1/SPP-LPPM/VI/2023), the integrated master to doctor scholarship program (PMDSU), and ITB Research 2023.

References

Brinchi, L., Cotana, F., Fortunati, E., Kenny, J.M., 2013. Production of Nanocrystalline Cellulose from Lignocellulosic Biomass: Technology and applications. *Carbohydrate polymers,* Volume 94(1), pp. 154–169

Budhi, Y.W., Fakhrudin, M., Culsum, N.T.U., Suendo, V., Iskandar, F., 2018. Preparation of Cellulose Nanocrystals from Empty Fruit Bunch of Palm Oil by using Phosphotungstic Acid Preparation of Cellulose Nanocrystals from Empty Fruit Bunch of Palm Oil by using Phosphotungstic Acid. *In:* IOP Conference Series: Earth and Environmental Science, Volume 105, p. 012063

Chen, X., Kuo, D.H., Lu, D., 2016. N-doped Mesoporous TiO_2 Nanoparticles Synthesized by using Biological Renewable Nanocrystalline Cellulose as Template for the Degradation of Pollutants under Visible and Sun Light. *Chemical Engineering Journal,* Volume 295, pp. 192–200

Culsum, N.T.U., Melinda, C., Leman, I., Wibowo, A., Budhi, Y.W., 2021. Isolation and Characterization of Cellulose Nanocrystals (CNCs) from Industrial Denim Waste using Ammonium Persulfate. *Materials Today Communications,* Volume 26, pp. 101817

Feng, S., Zhao, J., Bai, Y., Liang, X., Wang, T., Wang, C., 2020. Facile Synthesis of Mo-doped TiO_2 for Selective Photocatalytic CO_2 Reduction to Methane: Promoted H_2O Dissociation by Mo Doping. *Journal of CO_2 Utilization*. Volume 38, pp. 1–9

Harahap, M., Daulay, N., Zebua, D., Gea, S., 2023. Nanofiber Cellulose/Lignin from Oil Palm Empty Fruit Bunches and the Potential for Carbon Fiber Precursor Prepared by Wet-spinning. *Journal of CO_2 Utilization,* Volume 14, pp. 152–161

Hong, D., Lyu, L.M., Koga, K., Shimoyama, Y., Kon, Y., 2019. Plasmonic Ag@TiO_2 Core-Shell Nanoparticles for Enhanced CO_2 Photoconversion to CH_4. *ACS Sustainable Chemistry and Engineering*, Volume 7(23), pp. 18955–18964

Jiang, H., Wu, Y., Han, B., Zhang, Y., 2017. Effect of Oxidation Time on the Properties of Cellulose Nanocrystals from Hybrid Poplar Residues using the Ammonium Persulfate. *Carbohydrate Polymers*, Volume 174, pp. 291–298

Kumar, P.N., Das, A., Deepa, M., 2020. Nitrogen Doping of TiO_2 and Annealing Treatment of Photoanode for Enhanced Solar Cell Performance. *Journal of Alloys and Compounds*, Volume 832, p. 154880

Leung, A.C.W., Hrapovic, S., Lam, E., Liu, Y., Male, K.B., Mahmoud, K.A., Luong, J.H.T., 2011. Characteristics and Properties of Carboxylated Cellulose Nanocrystals Prepared from a Novel One-step Procedure. *Small*, Volume 7, pp. 302–305

Low, J., Cheng, B., Yu, J., 2017. Surface Modification and Enhanced Photocatalytic CO_2 Reduction Performance of TiO_2 : a Review. *Applied Surface Science*, Volume 392, pp. 658–686

Maimaiti, H., Awati, A., Yisilamu, G., Zhang, D., Wang, S., 2019. Synthesis and Visible-light Photocatalytic CO_2/H_2O Reduction to Methyl Formate of TiO_2 Nanoparticles Coated by Aminated Cellulose. *Applied Surface Science*, Volume 466, pp. 535–544

Marpongahtun, Andriayani, Muis, Y., Gea, S., Amaturrahim, S.A., Attaurrazaq, B., Daulay, A., 2023. Synthesis of Nitrogen-Doped Carbon Dots from Nanocrystalline Cellulose by Pyrolysis Method as Hg^{2+} Detector. *International Journal of Technology,* Volume 14(1), pp. 219–231

Martakov, I.S., Torlopov, M.A., Mikhaylov, V.I., Krivoshapkina, E.F., Silant'ev, V.E., Krivoshapkin, P. V, 2018. Interaction of Cellulose Nanocrystals with Titanium Dioxide and Peculiarities of Hybrid Structures Formation. *Journal of Sol-Gel Science and Technology,* Volume 88, pp. 13–21

Mase, N., Isomura, S., Toda, M., Watanabe, N., 2013. Micro and Nanobubble Based Strategy for Gas – Liquid – Solid Multiphase Re- actions : Palladium-Catalysed Hydrogenation of Carbon – Carbon Unsaturated Bonds. *Synlett,* Volume 24(17), pp. 2225–2228

Moon, R.J., Martini, A., Nairn, J., Simonsen, J., Youngblood, J., 2011. Cellulose Nanomaterials Review: Structure, Properties and Nanocomposites. *Chemical Society Reviews*, Volume 40(7), pp. 3941–3994

Mustapha, S., Ndamitso, M.M., Abdulkareem, A.S., Tijani, J.O., Shuaib, D.T., Ajala, A.O., Mohammed, A.K., 2020. Application of TiO_2 and ZnO Nanoparticles Immobilized on Clay in Wastewater Treatment: a Review. *Applied Water Science*, Volume 10, pp. 1–36

Restiawaty, E., Culsum, N.T., Nishiyama, N., Budhi, Y.W., 2022. Preparation, Characterization, and Surface Modification of Cellulose Nanocrystal from Lignocellulosic Biomass for Immobilized Lipase. *Fibers,* Volume 10(4), p. 33

Shao, B., Zhang, Y., Sun, Z., Li, J., Gao, Z., Xie, Z., Hu, J., Liu, H., 2022. CO2 Capture and in-situ Conversion: Recent Progresses and Perspectives. *Green Chemical Engineering,* Volume 3(3), pp. 189–198

Temesgen, T., Thuy, T., Han, M., Kim, T., Park, H., 2017. Micro and Nanobubble Technologies as a New Horizon for Water-treatment Techniques : A Review. *Advances in Colloid and Interface Science*, Volume 246, pp. 40–51

Ulatowski, K., Sobieszuk, P., Mróz, A., Ciach, T., 2019. Chemical Engineering & Processing : Process Intensification Stability of Nanobubbles Generated in Water using Porous Membrane System. *Chemical Engineering and Processing-Process Intensification,* Volume 136, pp. 62–71

Wibowo, A., Madani, H., Judawisastra, H., Restiawaty, E., Lazarus, C., Budhi, Y.W., 2018. An Eco-friendly Preparation of Cellulose Nano Crystals from Oil Palm Empty Fruit Bunches. *In:* IOP Conference Series: Earth and Environmental Science, Volume 105, pp. 012059

Xi, H., Xu, Y., Zou, W., Ji, J., Cai, Y., Wan, H., Dong, L., 2022. Enhanced Methanol Selectivity of $CuxO/TiO_2$ Photocatalytic CO_2 Reduction: Synergistic Mechanism of Surface Hydroxyl and Low-valence Copper Species. *Journal of CO_2 Utilization,* Volume 55, p. 101825

Yudha, S.S., Falahudin, A., Asdim, A., Han, J.I., 2020. Utilization of Dammar-Gum as a Soft Template in Titania Synthesis for Photocatalyst. *International Journal of Technology,* Volume 11(4), pp. 842–851

Zhang, X., Yuan, Z., Chen, J., Yang, G., Dionysiou, D.D., Huang, B., Jiang, Z., 2020. Enhanced CO_2 photoconversion activity of TiO_2 via double effect of CoPi as hole traps and high CO_2 capture. *Catalysis Today,* Volume 340, pp. 204–208